Ultrafast carrier dynamics and optical properties of nanoporous silicon at terahertz frequencies

J. R. Knab,[1,*] Xinchao Lu,[1,3] Felipe A. Vallejo,[1] Gagan Kumar,[2,4]
Thomas E. Murphy,[2] and L. Michael Hayden[1]

[1]*Department of Physics, University of Maryland Baltimore County, Baltimore, MD 21250, USA*
[2]*Institute for Research in Electronics & Applied Physics, University of Maryland College Park, College Park, MD 20742, USA*
[3]*Current Address: Institute of Microelectronics of Chinese Academy of Sciences, Beijing, 100029, China*
[4]*Current Address: Department of Physics, Indian Institute of Technology Guwahati, Guwahati, Assam-781039, India*
[*]*jrknab.31@gmail.com*

Abstract: We have investigated the broadband terahertz (THz) optical properties of nanoporous silicon samples with different porosities and the ultrafast carrier dynamics of photogenerated charge carriers in these materials. Following photoexcitation, we observe a fast carrier recovery time consisting of two dominant recombination processes with decay constants below ~10 ps. All samples exhibit initially low THz absorption that increases at higher frequencies, and is likely due to contributions from phonon bands and oxidation of the porous surface. The refractive index depends on porosity but shows little frequency dependence. These properties indicate that nanoporous silicon is a useful material for fast, ultrabroadband THz applications (e.g. intensity modulation).

©2014 Optical Society of America

OCIS codes: (300.6495) Spectroscopy, terahertz; (160.4236) Nanomaterials; (320.7130) Ultrafast processes in condensed matter, including semiconductors.

References and links

1. G. Bomchil, A. Halimaoui, and R. Herino, "Porous silicon: The material and its applications in silicon-on-insulator technologies," Appl. Surf. Sci. **41–42**, 604–613 (1989).
2. S. Labbé-Lavigne, S. Barret, F. Garet, L. Duvillaret, and J. L. Coutaz, "Far-infrared dielectric constant of porous silicon layers measured by terahertz time-domain spectroscopy," J. Appl. Phys. **83**(11), 6007–6010 (1998).
3. S.-Z. A. Lo and T. E. Murphy, "Nanoporous silicon multilayers for terahertz filtering," Opt. Lett. **34**(19), 2921–2923 (2009).
4. S.-Z. A. Lo, A. M. Rossi, and T. E. Murphy, "Terahertz transmission through p+ porous silicon membranes," Phys. Status Solidi A **206**(6), 1273–1277 (2009).
5. J. Xia, A. M. Rossi, and T. E. Murphy, "Laser-written nanoporous silicon ridge waveguide for highly sensitive optical sensors," Opt. Lett. **37**(2), 256–258 (2012).
6. V. S. Y. Lin, K. Motesharei, K.-P. S. Dancil, M. J. Sailor, and M. R. Ghadiri, "A porous silicon-based optical interferometric biosensor," Science **278**(5339), 840–843 (1997).
7. J. Diener, N. Kunzner, D. Kovalev, E. Gross, V. Y. Timoshenko, G. Polisski, and F. Koch, "Dichroic Bragg reflectors based on birefringent porous silicon," Appl. Phys. Lett. **78**(24), 3887–3889 (2001).
8. S.-Z. A. Lo, G. Kumar, T. E. Murphy, and E. J. Heilweil, "Application of nanoporous silicon substrates for terahertz spectroscopy," Opt. Mater. Express **3**(1), 114–125 (2013).
9. T. Matsumoto, T. Futagi, H. Mimura, and Y. Kanemitsu, "Ultrafast decay dynamics of luminescence in porous silicon," Phys. Rev. B Condens. Matter **47**(20), 13876–13879 (1993).
10. P. M. Fauchet, L. Tsybeskov, C. Peng, S. P. Duttagupta, J. von Behren, Y. Kostoulas, J. M. V. Vandyshev, and K. D. Hirschman, "Light-emitting porous silicon: materials science, properties, and device applications," IEEE J. Sel. Top. Quantum Electron. **1**(4), 1126–1139 (1995).
11. M. Rahm, J.-S. Li, and W. J. Padilla, "THz Wave Modulators: A brief review on different modulation techniques," J. Infrared Milli. Terahz. Waves **34**(1), 1–27 (2013).
12. H.-T. Chen, W. J. Padilla, J. M. O. Zide, S. R. Bank, A. C. Gossard, A. J. Taylor, and R. D. Averitt, "Ultrafast optical switching of terahertz metamaterials fabricated on ErAs/GaAs nanoisland superlattices," Opt. Lett. **32**(12), 1620–1622 (2007).
13. L. Fekete, F. Kadlec, P. Kužel, and H. Němec, "Ultrafast opto-terahertz photonic crystal modulator," Opt. Lett. **32**(6), 680–682 (2007).

14. T. Kleine-Ostmann, P. Dawson, K. Pierz, G. Hein, and M. Koch, "Room-temperature operation of an electrically driven terahertz modulator," Appl. Phys. Lett. **84**(18), 3555–3557 (2004).
15. J. Kyoung, M. Seo, H. Park, S. Koo, H. S. Kim, Y. Park, B.-J. Kim, K. Ahn, N. Park, H.-T. Kim, and D.-S. Kim, "Giant nonlinear response of terahertz nanoresonators on VO_2 thin film," Opt. Express **18**(16), 16452–16459 (2010).
16. J. Shu, C. Qiu, V. Astley, D. Nickel, D. M. Mittleman, and Q. Xu, "High-contrast terahertz modulator based on extraordinary transmission through a ring aperture," Opt. Express **19**(27), 26666–26671 (2011).
17. H. K. Yoo, C. Kang, Y. Yoon, H. Lee, J. W. Lee, K. Lee, and C.-S. Kee, "Organic conjugated material-based broadband terahertz wave modulators," Appl. Phys. Lett. **99**(6), 061108 (2011).
18. B. Sensale-Rodriguez, R. Yan, M. M. Kelly, T. Fang, K. Tahy, W. S. Hwang, D. Jena, L. Liu, and H. G. Xing, "Broadband graphene terahertz modulators enabled by intraband transitions," Nat Commun **3**, 780 (2012).
19. P. D. Cunningham and L. M. Hayden, "Carrier dynamics resulting from above and below gap excitation of P3HT and P3HT/PCBM investigated by optical-pump terahertz-probe spectroscopy,," J. Phys. Chem. C **112**(21), 7928–7935 (2008).
20. D. J. Cook and R. M. Hochstrasser, "Intense terahertz pulses by four-wave rectification in air," Opt. Lett. **25**(16), 1210–1212 (2000).
21. N. Karpowicz, J. Dai, X. Lu, Y. Chen, M. Yamaguchi, H. Zhao, X.-C. Zhang, L. Zhang, C. Zhang, M. Price-Gallagher, C. Fletcher, O. Mamer, A. Lesimple, and K. Johnson, "Coherent heterodyne time-domain spectrometry covering the entire "terahertz gap"," Appl. Phys. Lett. **92**(1), 011131 (2008).
22. C. V. McLaughlin, L. M. Hayden, B. Polishak, S. Huang, J. Luo, T.-D. Kim, and A. K. Y. Jen, "Wideband 15 THz response using organic electro-optic polymer emitter-sensor pairs at telecommunication wavelengths," Appl. Phys. Lett. **92**(15), 151107 (2008).
23. F. A. Hegmann, O. Ostroverkhova, and D. G. Cooke, "Probing Organic Semiconductors with Terahertz Pulses," in *Photophysics of Molecular Materials: From Single Molecules to Single Crystals*, G. Lanzani, ed. (Wiley-VCH Verlag GmbH & Co. KGaA, Weinheim, FRG, 2006).
24. T. Nozokido, H. Minamide, and K. Mizuno, "Modulation of submillimeter wave radiation by laser-produced free carriers in semiconductors," Electron. Comm. Jpn. Pt. II **80**(6), 1–9 (1997).
25. V. Y. Timoshenko, T. Dittrich, V. Lysenko, M. G. Lisachenko, and F. Koch, "Free charge carriers in mesoporous silicon," Phys. Rev. B **64**(8), 085314 (2001).
26. D. G. Cooke, A. N. MacDonald, A. Hryciw, J. Wang, Q. Li, A. Meldrum, and F. A. Hegmann, "Transient terahertz conductivity in photoexcited silicon nanocrystal films," Phys. Rev. B **73**(19), 193311 (2006).
27. P. U. Jepsen, W. Schairer, I. H. Libon, U. Lemmer, N. E. Hecker, M. Birkholz, K. Lips, and M. Schall, "Ultrafast carrier trapping in microcrystalline silicon observed in optical pump–terahertz probe measurements," Appl. Phys. Lett. **79**(9), 1291–1293 (2001).
28. H. Tang, L.-G. Zhu, L. Zhao, X. Zhang, J. Shan, and S.-T. Lee, "Carrier dynamics in Si nanowires fabricated by metal-assisted chemical etching," ACS Nano **6**(9), 7814–7819 (2012).
29. L. Duvillaret, F. Garet, and J. L. Coutaz, "A reliable method for extraction of material parameters in terahertz time-domain spectroscopy," IEEE J. Sel. Top. Quantum Electron. **2**(3), 739–746 (1996).
30. A. K. W. Abdullah, K. A. Maslin, and T. J. Parker, "Observation of two-phonon difference bands in the FIR transmission spectrum of Si," Infrared Phys. **24**(2-3), 185–188 (1984).
31. F. A. Johnson, "Lattice Absorption Bands in Silicon," Proc. Phys. Soc. **73**(2), 265–272 (1959).
32. H. R. Philipp, "Silicon Dioxide (SiO_2) (Glass)," in *Handbook of Optical Constants of Solids,* E. D. Palik, ed. (Academic Press, 1997).

1. Introduction

Nanoporous silicon consists of a sponge-like network of nanometer-scale pores (<100 nm) formed by electrochemical etching of doped silicon substrates [1]. The size of the pores, as well as the porosity of the system, can be readily controlled in the fabrication process. The introduction of nanometer-scale pores can yield optical and electrical properties that are dramatically different from the bulk silicon from which the same is formed. For example, even though the silicon substrates are heavily doped and hence conductive, the porous samples studied here are shown to be largely transparent in the terahertz regime.

At terahertz (THz) frequencies, the frequency-dependent refractive index was reported to decrease in porous silicon compared to its bulk precursor [2], and could be tuned by simply altering the porosity. The ability to engineer the effective dielectric constant by adjusting the porosity, and to construct complex multilayer porous structures on a single silicon substrate provides unparalleled flexibility in the fabrication of THz components [3]. In addition, it has been shown that the attenuation of THz light in the 0.1-2.5 THz range is quite low (< 4 cm^{-1}) [4], making nanoporous silicon an ideal material for use in applications where low insertion loss is important.

The possibility to modify the refractive index, along with the large surface-to-volume ratio of nanoporous silicon, has led to a number of interesting applications, including but not

limited to chemical sensors [5], biological sensors [6], optical components [3,7], and substrate material [8]. The latter can be used to study, e.g., nanoconfined systems, or for a broad array of spectroscopy and sensing applications that call for liquid or gas penetration directly into a dielectric medium. An example of the latter could be a THz biosensor, where the pores could be functionalized with a binding medium, thus greatly improving the interaction area between THz light and the material being detected or analyzed.

Fast carrier recombination times have been reported for nanoporous silicon in time-resolved measurements, such as photoluminescence decay [9] and photoinduced absorption [10]. Though these types of measurements do not directly probe the carrier dynamics, they do provide an indication that nanoporous silicon may be a strong candidate for a broadband, THz intensity modulator. Several types of THz modulators have been proposed [11], including modulators based on metamaterials [12], photonic crystals [13], electrically-driven two-dimensional electron gas [14], VO_2 insulator-to-metal phase transition [15], free-carrier modulation of extraordinary optical transmission [16], organic materials [17], and graphene [18]. Ideally, a modulator should have a fast response time and strong signal modulation. In addition, broadband operation (versus single-frequency response), ease of fabrication, and polarization independence are also desirable characteristics. The aforementioned modulators and others like them typically excel in either speed or modulation depth, or they only operate at specific frequencies.

In order to consider nanoporous silicon for use as an all-optical, broadband THz modulator or for any other application, the dynamics of photogenerated carriers as well as the optical properties of nanoporous silicon must be evaluated. In this work, we directly measure ultrafast photocarrier recombination times using optical-pump THz-probe (OPTP) measurements. As we will show, nanoporous silicon possesses an ultrafast response *and* excellent modulation depth, making it an excellent candidate material for an all-optical THz modulator. We also assess the broadband optical properties of nanoporous silicon across almost the entire THz band (2.0-10.0 THz). Using terahertz time-domain spectroscopy (THz-TDS), we measure a relatively low absorption coefficient at lower frequencies and a flat refractive index. However, absorption loss becomes more prominent at higher frequencies. This may limit the usefulness of nanoporous silicon in applications where low insertion loss is desired (e.g. THz filters), but could still allow use below ~10 THz. These favorable optical properties show that nanoporous silicon can be employed in a number of THz optical or photonic applications over a very wide frequency range, and offer another distinct advantage for a THz modulator formed from this material.

2. Sample preparation and experimental technique

Free-standing, nanoporous silicon membranes are fabricated via electrochemical etching of *p*-type (boron-doped) silicon wafers [4]. The resistivity of each wafer is 1–5 mΩ-cm, corresponding to a dopant concentration of ~10^{20} cm^{-3}. The etching is performed in the dark, using an electrolyte mixture of hydrofluoric acid, water, and ethanol, in a volume ratio of 1:1:2. The electrochemical current density is adjusted in order to achieve the desired porosity and refractive index. In order to separate the porous layer from the substrate, a strong current pulse of 1 A/cm^2 is applied for 20 seconds, resulting in a freestanding porous membrane. The sample is then oxidized in a rapid thermal annealer, at a temperature of 400°C for 5 minutes, in order to passivate the silicon surfaces. Scanning electron microscope images of a freestanding nanoporous silicon sample, which was fabricated using this process, are shown in Fig. 1.
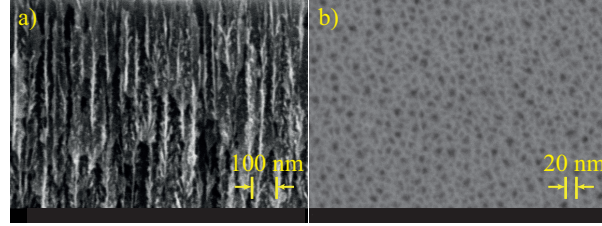
Fig. 1. Scanning electron microscope images of a typical nanoporous silicon sample. (a) cross-sectional view showing vertically oriented pores traversing the sample. (b) top view of the sample. Typical pore sizes are 10-30 nm.

The samples are a few hundred microns thick, and the pores, which are distributed throughout the sample, have an estimated diameter of 10-30 nm. The pores are vertically oriented and traverse the entire sample. The samples are all 1.0 cm in diameter.

Optical-pump terahertz probe (OPTP) and THz-TDS measurements were performed using a standard THz setup, details of which are described elsewhere [19]. The laser used to generate and detect THz light, as well as to optically excite the nanoporous silicon samples is a regenerative Ti:Sapphire amplifier having a central wavelength of ~800 nm, pulse energy of ~3 mJ, 1.0 kHz repetition rate and ~25 fs pulse duration. THz fields were generated by mixing the fundamental and second harmonic of the laser in an air-plasma [20]. THz light was focused on the sample at normal incidence, and the transmitted field was detected using free space, electro-optic sampling. For the OPTP measurements, a 2.0 mm-thick, (110) ZnTe crystal was used to detect the THz light. In order to detect broader bandwidth in the spectroscopic measurements, we utilized either THz air-biased coherent detection [21] or an electro-optic polymer sensor [22]. The incident THz radiation was linearly polarized in the direction perpendicular to the pore axes. The entire setup was enclosed in a box and purged with dry air.

In order to assess the effect of porosity on carrier dynamics, three samples having different porosities were studied. For each sample, the effective refractive index, n, was measured using THz-TDS and the porosity was estimated using the Bruggeman effective medium approximation:

$$(1-p)\frac{\left(n_{Si}^2 - n^2\right)}{n_{Si}^2 + 2n^2} + p\frac{\left(n_{air}^2 - n^2\right)}{n_{air}^2 + 2n^2} = 0 \qquad (1)$$

where p is the air-pore volume fraction, n_{Si} ~3.4 is the index of silicon and n_{air} ~1 is the refractive index of air. The measured refractive indices, estimated porosities and sample thicknesses are given in Table 1.

Table 1. Nanoporous silicon sample parameters

n	Porosity, p	Thickness (μm)
1.32	0.798	362
1.46	0.735	281
1.55	0.698	170

The samples were photoexcited with an 800 nm pump beam (fluence = 3.6x10^{15} photons/cm²/pulse, 0.9 mJ/cm²/pulse), which promotes electrons into the conduction band of nanoporous silicon. In order to estimate the absorption depth at 800 nm, we measured the absorption spectrum for all samples using a Perkin-Elmer Lambda 3B Spectrophotometer. Though this did not account for reflected or scattered light, we can estimate the absorption depth from the measured spectra to be ~70-80 μm. By fixing the synchronously generated, THz probe beam at the peak of the transmitted THz electric field and adjusting the relative delay of the 800 nm pump beam, we measure the average THz transmission change across the bandwidth contained in the THz pulse, as a function of time. Since the transmission change

depends on the number density of the mobile, photoexcited charge carriers [23], the time evolution of the system is directly monitored as it returns to equilibrium. Being directly sensitive to the photoexcited charge carriers is a distinct advantage of using OPTP measurements to probe carrier dynamics, as opposed to other all-optical techniques, such as time-resolved photoluminescence, where the carrier dynamics is indirectly inferred. The pump beam propagated nearly collinearly with the THz probe, which was normally incident upon the samples.

3. Results and discussion

The time-dependent, THz transmission changes for all samples, normalized to the field transmitted through the unexcited samples, is plotted in Fig. 2.
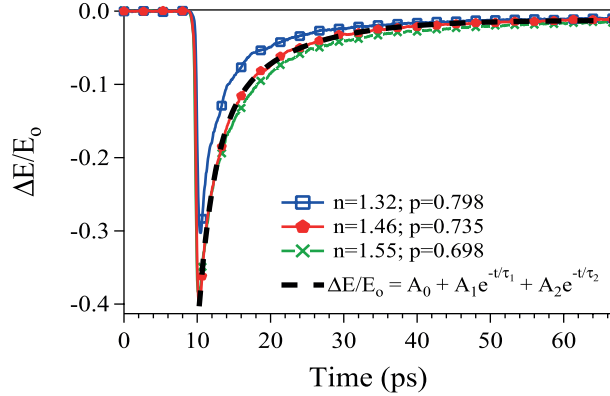

Fig. 2. Change in peak THz transmission as a function of time after excitation for nanoporous Si samples with different porosities. The samples were photoexcited using an 800 nm pump beam with a fluence of 3.6×10^{15} photons/cm^2 (0.9 mJ/cm^2) per pulse. The differential transmission was normalized to the transmission through the unexcited sample.

The sharp decrease in the transmission coincides with the arrival of the pump pulse and indicates that a large density of photoexcited charge carriers has been created. This occurs on a timescale of ~1.5 ps for each sample. The recombination of the electron-hole pairs can be described via three decay channels, and can be fit with the following expression: $\Delta E / E_0 = A_0 + A_1 e^{-t/\tau_1} + A_2 e^{-t/\tau_2}$. The characteristic recombination time is given by τ_i, and the A_i coefficients are proportional to the number of carriers participating in a particular recombination process. The black dashed line in Fig. 2 is a fit for the $n = 1.46$ sample and is an exemplar of fits for the other samples. The time for the differential THz signal to recover to a small background level is remarkably fast, considering that carrier recombination times in, e.g., bulk high-resistivity Si, are typically many orders of magnitude slower, on the order of several hundred microseconds [24]. Given the large surface to volume ratio in these nanoporous silicon samples, it is probable that the fast recovery time observed here is due to recombination mediated by surface states. These are likely amphoteric defect states, present at the Si/SiO$_2$ interface [25], which provide alternative pathways for carrier relaxation back to the valence band. Interestingly, it was shown that the indirect nature of the bandgap, which is responsible for the long-lived carriers in bulk silicon, is preserved in nanoporous silicon [10]. A constant term (A_0) is included in the expression used to fit the data shown in Fig. 2, to represent the small percentage of long-lived photoexcited carriers that slowly recombine beyond the limit of our measurement window, presumably via bulk-like states. There are two fast decay processes, indicated by τ_1 and τ_2. These relaxation times are approximately the same for each channel over the range of porosities studied here: τ_1~2 ps and τ_2~10 ps [see Fig. 3]. The proportion of carriers participating in either decay channel, however, changes as a function of porosity, as shown in the inset of Fig. 3. The fraction of carriers that recombine via the faster decay channel (A_1) increases with porosity, while the fraction in the slower

decay channel (A_2) decreases. Higher porosity implies increased surface area in the nanoporous silicon structure and thus a greater density of available surface states. This provides a clue about the nature of the defects, though more detailed study is needed in order to determine the exact physical origin of the fast and slower decay channels.
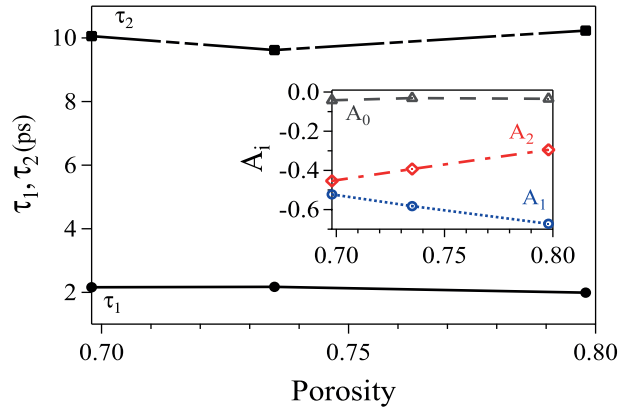

Fig. 3. Relaxation times, τ_i, and fit parameters, A_i (inset), as a function of porosity. Data are from fits to differential transmission data shown in Fig. 2, which have been normalized to their respective minimum values ($\sum_i A_i = -1$).

Surface states are integral in determining the carrier recombination time in systems with high surface to volume ratios like nanoporous silicon. For example, in an OPTP study of nano-*crystalline* silicon [26], decay times were reported that became faster as nanocluster size decreased, presumably due to an increased surface to volume ratio and fast carrier trapping in Si/SiO$_2$ interface states. In another OPTP study of *micro-crystalline* silicon [27], a fast initial decay time of ~0.7 ps was reported, corresponding to trapping of a fraction of the mobile carriers. Following this, the recovery became very slow, possibly due to saturation of trap/defect states, and was outside the range of their experimental window (6 ps). While we do not observe saturation of the overall recovery for nanoporous silicon at the fluence level used in our studies, initial results from measurements of the fluence dependence in another sample (not shown) exhibit an increase in τ_1, possibly due to saturation in that decay channel. In contrast to the fast recovery exhibited by our samples, a recent OPTP study of silicon nano*wires* [28] (diameter = 250-300 nm) reported a carrier lifetime of 700 ps. This relatively longer lifetime was attributed to the high quality, bulk-like cores of the wires, with carrier trapping in surface states of the wires reducing the carrier lifetime relative to that in bulk silicon. The lifetime in Si nanowires is substantially longer than what we have measured for nanoporous silicon, probably due to the fact that the silicon portions in our samples are likely only tens of nanometers wide and the surface to volume ratio is larger. Perhaps through manipulation of the surface states in nanoporous silicon, via e.g., different surface passivation, the recombination time can be further decreased. Remarkably, a few of our nanoporous silicon samples have shown a nearly complete recovery within ~*5 ps*, possibly due to different fabrication conditions. This represents a significant performance enhancement, though further studies are required in order to identify the factors that contribute to these fast recovery times.

Nanoporous silicon exhibits not only an ultrafast response, but also a good modulation depth, both of which are important characteristics that are highly desirable in an all-optical THz modulator. We were able to achieve ~40% modulation depth with a nearly complete transmission recovery in a few tens of picoseconds. This is likely due to a large density of surface states, as well as the penetration depth of the 800 nm pump beam. This behavior satisfies the performance requirements for both speed *and* sizable signal modulation. One might expect that the modulation depth should change with porosity. The data shown in

Fig. 2, however, do not exhibit a definitive trend. Among other things, this can be attributed to differences in sample homogeneity, along with different photocarrier generation efficiencies and carrier mobilities. Additional measurements over a larger sample set, containing a greater range of porosities will be necessary in order to discern a trend.

Nanoporous silicon will also be advantageous since it can be used over a broad bandwidth. In order to ascertain whether the favorable optical properties observed at lower frequencies [2–4] (i.e. low attenuation and tunable refractive index) extend beyond 2.5 THz, we have measured the broadband, THz spectral response for the nanoporous silicon samples [Fig. 4]. For each sample, we measured a reference THz field transmitted through dry air. The refractive index and absorption coefficient were obtained using the minimization algorithm of Duvillaret *et al.* [29].
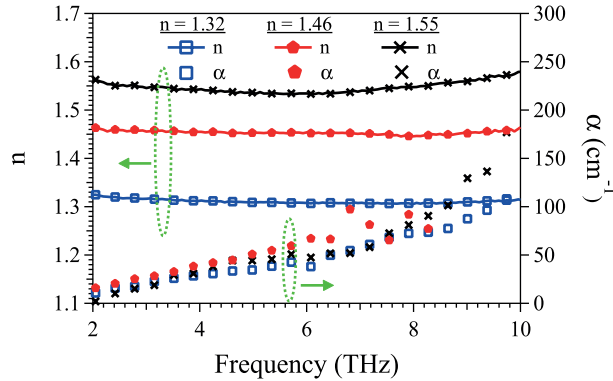

Fig. 4. Broadband THz refractive index, *n* (left axis), and absorption coefficient, *α* (right axis), for nanoporous silicon samples. The *α*-data for the *n* = 1.46 sample only extend to 8.3 THz due to a reduced dynamic range at higher frequencies for the polymer sensor used in those measurements.

One of the interesting features of nanoporous silicon is that it is relatively transparent throughout the THz regime, considering that it was formed from highly-doped silicon, which would ordinarily be opaque at THz frequencies. All samples have a relatively featureless, broadband response out to ~10 THz, beyond which the THz light is almost completely attenuated. The increasing attenuation as a function of frequency is consistent with recently reported FTIR transmission data [8]. We do not expect a large contribution to the attenuation from scattering loss, since the wavelengths of the THz light used in this work (30 μm - 150 μm) are many orders of magnitude larger than the average pore diameter. In addition, we do not expect a scattering contribution due to surface roughness. Surface profiles from AFM measurements (not shown) of similarly made samples exhibit rms surface roughness ranging from 13 nm to 52 nm, values which are much smaller than the THz wavelengths. On the other hand, several weak phonon bands at 3.66 THz [30], 4.88 THz [30], and 11.17 THz [31] might partly contribute to the attenuation. The tails of a higher frequency band at 16.99 THz [31], as well as a stronger phonon mode at 18 THz may also affect the high-frequency response. Note that at the lower frequencies, however, we do not directly observe the signature of any strong phonon resonances. Since these phonon modes are weak, their contributions to the dielectric response are most likely small. Contributions from free-carrier absorption are also not likely, as the resistivity of the material has increased by several orders of magnitude during the fabrication process, resulting in an insulating dielectric material [4]. An additional, stronger contribution to the attenuation likely originates from the SiO_2 layer. For transmission measurements of bulk silicon wafers, one would not normally observe the influence of a very thin layer of SiO_2. However, the nanoporous silicon samples have considerably more surface area (several hundred m^2/cm^3), and thus more oxide with which the THz light interacts. In samples that are a few hundred micrometers thick, this equates to non-negligible volumes of SiO_2. The attenuation due to SiO_2 increases with frequency until it reaches a peak at a strong

lattice mode around 14 THz [32]. The combination of this, along with our decreasing dynamic range can explain the cutoff of the usable THz spectrum around 10 THz for all three samples. In general, no clear trend in the sample attenuation is observed as a function of porosity, though in principle, one would expect the least porous sample to have lower absorption loss by virtue of the fact that it has more bulk Si. However, a broader range of porosities must be studied in order to verify this.

The refractive indices of the nanoporous silicon samples studied here [Fig. 4] are much lower than for bulk silicon (n ~3.4) and are easily tuned by modifying the sample porosity, where the index decreases as the porosity (and thus void volume) increases. The tunability of the index and low absorption at lower frequencies is similar to previously reported THz-TDS results in the 0.1-2.5 THz range [2, 4]. The relatively flat frequency-dependence of the refractive indices reported here extends throughout our 10 THz measurement window, and is also observed at lower frequencies (not shown). The lower attenuation of THz light (in the range below 7 THz) and tunable index of nanoporous silicon make it a useful platform for broadband THz applications. At higher frequencies, however, the feasibility of using nanoporous silicon for the aforementioned applications will be limited due to the much greater attenuation of THz light.

4. Conclusions

Our results show nanoporous silicon to be a versatile and useful material for ultrabroadband THz applications. The ultrafast carrier recovery time, favorable modulation depth and broadband optical properties make nanoporous silicon a strong candidate for an all-optical THz modulator. This material is relatively inexpensive and easy to fabricate, and the fabrication process can be easily up-scaled for large-scale production. Nanoporous silicon is also structurally simple, since deposition of electrodes, apertures or other structures is not necessary for a functioning modulator. To our knowledge, there are not many modulator materials that share all of these characteristics. The low attenuation and relatively flat refractive index extends the useful frequency range for applications to ~7 THz, depending on how much loss is acceptable for a given application. These favorable ultrabroadband optical properties indicate that nanoporous silicon can be utilized in THz optical and photonic components throughout the THz frequency range. This will facilitate development of THz components made from this material, such as THz filters [3], in this underexploited part of the electromagnetic spectrum.

Acknowledgments